Journal of Materials Chemistry A

PAPER

View Article Online
View Journal | View Issue

Cite this: *J. Mater. Chem. A*, 2015, **3**, 6351

The vapour phase detection of explosive markers and derivatives using two fluorescent metal–organic frameworks†

Monika Jurcic,[ab] William J. Peveler,[ab] Christopher N. Savory,[c] David O. Scanlon,[cd] Anthony J. Kenyon[e] and Ivan P. Parkin*[b]

Received 21st October 2014
Accepted 17th February 2015

DOI: 10.1039/c4ta05638h

www.rsc.org/MaterialsA

Two fluorescent metal–organic frameworks (MOFs) [Zn(dcbpy)(DMF)]·DMF and [Dy(dcbpy)(DMF)$_2$(NO$_3$)] (dcbpy = 2,2′-bipyridine-4,4′-dicarboxylate) were synthesised solvothermally and structurally characterised. Uniform shape and sized microcrystals of [Zn(dcbpy)(DMF)]·DMF were also produced using microwave synthesis. The frameworks give organic linker-based fluorescence emission and demonstrate very different detection capabilities towards the explosive taggant 2,3-dimethyl-2,3-dinitrobutane (DMNB) and trinitrotoluene (TNT) derivatives; 2,4-dinitrotoulene (2,4-DNT), nitrobenzene (NB) and *para*-nitrotoluene (*p*-NT). These differences are attributed to the variation in the overall framework architecture between the two MOFs. This paper reiterates the key importance of MOF porosity in sensing applications, and highlights the value of uniform microcrystals to sensitivity.

1 Introduction

The increase in terrorism related explosive attacks in recent years has led to the urgent need in detection methods that successfully identify explosives or explosive related materials on a person, surface or as a vapour.[1] Particularly desired are vapour phase detection methods that have good sensitivity, selectivity, reproducibility, rapid response times and instrumental portability and stability.[2] The difficulty in the detection of explosives arises from their extremely low vapour pressures, especially in the case for commercial explosives such as 2,4,6,-trinitrotoluene (TNT). As a result, explosive sensing methods frequently detect precursors or derivatives of explosives.[3] 2,4-Dinitrotoluene (2,4-DNT), an unavoidable by-product in the manufacturing of TNT, has a much higher vapour pressure than its parent compound, and thus is often a focal point for TNT sensing (Table 1). Other precursors for TNT include 2,6-dinitrotoluene, *para*-nitrotoluene (*p*-NT) and nitrobenzene (NB), all of which are markers of the presence of explosive materials. Furthermore, dinitrotoluenes and nitrobenzene are known toxic, organic pollutants that are frequently discharged into the environment by industrial production processes, and the detection of these materials is of paramount importance.[4] Another taggant of interest is 2,3-dimethyl-2,3-dinitrobutane (DMNB).[5] This material is mandated by law to be included in military plastic explosives formulations for detection purposes.[6]

Traditional explosive detection methods include sniffer dogs,[7] as well as instrumental techniques such as gas chromatography-mass spectrometry,[8] ion mobility spectrometry and Raman spectroscopy.[9,10] Although such instrumental methods have proven extremely effective, they are often very expensive and not readily portable. New chemical sensing tools are therefore being explored for the detection of explosives in the field. Chemical sensors such as electronic noses,[11,12] biological assays and colorimetric sensors have attracted particular attention.[13,14] In addition, numerous fluorescent-based chemical sensors have recently been explored.[15–17] Fluorescent conjugated polymers have dominated this field, producing some of the technologies used by the security industry.[18]

Metal–organic frameworks (MOFs), a relatively new class of porous and crystalline materials,[19] have demonstrated promise in a number of applications including gas storage and separation,[20–22] catalysis,[23–25] and drug delivery.[26–30] More recently MOFs are emerging as auspicious candidates for fluorescence-based explosives detection owing to their ease of synthesis, tuneability of pore size and functionality, high surface areas and surface chemistry, all of which make MOFs excellent luminescent explosives-detecting materials.[31–34]

[a]Department of Security and Crime Science, University College London, London, WC1H 9EZ, UK

[b]Department of Chemistry, University College London, London, WC1H 0AJ, UK. E-mail: i.p.parkin@ucl.ac.uk

[c]Kathleen Lonsdale Materials Chemistry, Department of Chemistry, University College London, London WC1H 0AJ, UK

[d]Diamond Light Source Ltd., Diamond House, Harwell Science and Innovation Campus, Didcot, Oxfordshire OX11 0DE, UK

[e]Department of Electronic & Electrical Engineering, University College London, London, WC1E 7JE, UK

† Electronic supplementary information (ESI) available: Additional crystallographic, PXRD, TGA and fluorescence data. CCDC 992713 and 1026241. For ESI and crystallographic data in CIF or other electronic format see DOI: 10.1039/c4ta05638h

Table 1 Table of explosive vapour pressures

Name	Class	Vapour pressure at 25 °C/Torr
2,4,6-Trinitrotoluene (TNT)[35]	Nitroaromatic military explosive	5.5×10^{-6}
2,4-Dinitrotoluene (2,4-DNT)[35]	Nitroaromatic TNT derivative/toxic organic pollutant	2.6×10^{-4}
2,6-Dinitrotoluene (2,6-DNT)[35]	Nitroaromatic TNT derivative/toxic organic pollutant	6.2×10^{-4}
para-Nitrotoluene (*p*-NT)[35]	Nitroaromatic TNT derivative/proposed toxic organic pollutant	4.9×10^{-2}
Nitrobenzene (NB)[35]	Nitroaromatic TNT derivative/toxic organic pollutant	3.1×10^{-1}
2,3-Dimethyl-2,3-dinitrobutane (DMNB)[6]	Nitroaliphatic explosives taggant	2.1×10^{-3}

A number of MOFs have demonstrated successful detection of explosives based on fluorescence-quenching.[36] The high fluorescence intensities of certain MOFs attenuate on exposure to explosives or explosive-related analytes, yielding a detectable intensity change. Pioneering work within this field was performed by Li *et al.* who demonstrated the sensitive detection of DMNB and 2,4-DNT in the vapour phase.[37] This work inspired a number of other researchers who subsequently demonstrated the successful detection of explosives, with some selectivity, using zinc,[38–43] cadmium,[44–46] lithium,[47] indium,[48] europium,[49–52] and terbium containing metal–organic frameworks.[53] However, the majority of the published research reports the detection of explosives using MOFs through solution-based titrations. Although this allows for excellent proof-of-concept experiments, it limits the use of these materials for portable in-field detection of explosives.

Here we report two novel highly fluorescent metal–organic frameworks [Zn(dcbpy)(DMF)]·DMF (**1**) and [Dy(dcbpy)(DMF)$_2$(NO$_3$)] (**2**) (dcbpy = 2,2′-bipyridine-4,4′-dicarboxylate; DMF = dimethylformamide) for the vapour-phase detection of explosive derivatives and related compounds.

Owing to the constantly evolving explosive threat, we believe that the ease at which MOFs can be tailored (through judicial choice of organic linker and metal), for the potential targeting of a system towards a particular analyte, adds great value to their use within the security industry. Thus, we have explored how alteration of one component of our particular MOF system can effect its sensing towards specified nitroaromatic and nitroalipatic compounds. MOFs **1** and **2** have both been constructed from the same electron rich organic ligand H$_2$dcbpy, but vary in metal composition. As a consequence, the frameworks demonstrate different architectures and sensing towards nitroaromatic and nitroaliphatic explosive analytes. The use of a lanthanide was employed with aim to increase the system's luminescence. This is to our knowledge the first dysprosium-based MOF reported for the successful sensing of explosives related analytes. Finally we demonstrate a rapid syntheses of uniform [Zn(dcbpy)(DMF)]·DMF microcrystals (**1M**) *via* microwave synthesis, and show how these homogenous microcrystals give increased sensing sensitivities compared to their solvothermally synthesised counterparts.

2 Experimental

2.1 Synthesis

Synthesis of [Zn(dcbpy)(DMF)]·DMF (1). MOF **1** was synthesised *via* a typical solvothermal method. $Zn(NO_3)_2 \cdot 6H_2O$ (0.4 mmol, 119.0 mg) and H$_2$dcbpy (0.4 mmol, 97.8 mg) were dissolved in DMF (15 mL) with stirring in a glass vial. The vial was sealed and placed in an oven set to 100 °C for 6 days, affording the colourless rectangular plate-like crystals of **1**.

Microwave synthesis of [Zn(dcbpy)(DMF)]·DMF (1M). $Zn(NO_3)_2 \cdot 6H_2O$ (0.2 mmol, 60.0 mg) and H$_2$dcbpy (0.4 mmol, 48.8 mg) were dissolved in DMF (12 mL) in a glass vial under stirring and a low heat of approximately 40 °C for approximately 10 minutes. After the majority of the contents had dissolved, 3 mL of the cloudy reactant solution was syringed into a new glass vial, this glass vial was sealed and placed in a 700 W microwave operating at 40% power output. The sample was irradiated initially for 30 s, followed by three more 30 s cycles. This afforded a clear solution and a microcrystalline MOF precipitate (ESI†).

Synthesis of [Dy(dcbpy)(DMF)$_2$(NO$_3$)] (2). Metal–organic framework **2** was synthesised solvothermally as for **1**. $Dy(NO_3)_3 \cdot 5H_2O$ (0.4 mmol, 175.6 mg) and H$_2$dcbpy (0.4 mmol, 97.9 mg) were dissolved in DMF (15 mL) with stirring in a glass vial. The vial was sealed and placed in an oven set to 100 °C for 6 days, affording pale pink rhomboidal crystals of **2**.

2.2 Washing regimes to afford active MOFs

The crystals of MOFs **1**, **1M** and **2** were immersed in solutions of methanol, followed by dichloromethane and subsequently dried under vacuum, yielding 'active MOFs' **1′**, **1M′** and **2′**.

2.3 Generation of MOF thin films

Thin films of **1′**, **1M′** and **2′** were prepared prior to vapour phase sensing experimentation. The films were fabricated on microscope slides, onto which, finely ground crystals of the MOF were compacted until firmly in place and any excess residue was tapped from the slides, giving the MOF thin films of typically 10 μm thickness (ESI†).

2.4 Fluorescence sensing methodology

Each thin film's fluorescence was measured initially three times and averaged, giving a stable base line (intensity = I_0), ensuring that any quenching of the system observed was not a result of MOF material loss. Then after exposure to the vapour headspace of a particular analyte for 10 s the fluorescence was measured (I). The films were further exposed to analytes for 30 s, 60 s, 120 s and 300 s, and the fluorescence intensity was re-measured after each time period. Analyte vapours of DMNB, 2,4-DNT, *p*-NT and NB were generated by depositing small amounts of the analytes into sealed tubes, creating a static headspace. The MOF-thin films were rapidly placed inside the sealed tubes for fixed amounts of time during the sensing procedure.

2.5 Characterisation instrumentation

Fluorescence was measured on an Edinburgh Instruments time-correlated single photon counter (TCSPC) with laser excitation at 405 nm and emission measured between 420 and 750 nm. Powder X-ray diffraction patterns were collected on an STOE Stadi-P transmission diffractometer system, CuKα (λ = 1.54184 Å) radiation source, operating at 40 kilowatts and 30 miliamperes. SEM images were collected on a field emission Jeol 6700F FEG SEM operating at 5 kV. Thermogravimetric analyses of the samples were performed on a Netzsch Jupiter thermal gravimetric analyser. The samples were purged with air and ramped from room temperature to 500 °C at 10 °C min^{-1}. Microwave synthesis was undertaken using a conventional microwave oven with a 700 W and 2450 MHz output. The microwave was operated at a 40% power output. Single crystal X-ray diffraction data for MOFs **1** and **2** were collected at 150.0(10) K on a SuperNova, Dual, Cu at zero, Atlas diffractometer, with CuKα (λ = 1.54184 Å) radiation. Using Olex2,[54] the structures were solved with the Superflip[55] structure solution program using charge flipping and refined with the ShelXL[56] refinement package using least squares minimisation.

3 Results and discussion

3.1 Characterisation

Single crystal X-ray diffraction analysis on [Zn(dcbpy)(DMF)]·DMF **1** disclosed a three-dimensional framework belonging to the monoclinic space group $P2_1/n$. The overall architecture of this MOF is governed by the cyclic secondary building units (SBUs) that are formed. The eight-membered SBUs located in this MOF are constructed from the monodentate carboxylates of two dcbpy ligands, two centrosymmetrically related dcbpy ligands (coordinated to two zinc metals through the N-donor moieties) and two DMF solvent molecules. A representation of the SBU is given in Fig. 1a.

The SBU nodes are further linked to other secondary building units through the carboxylate and N-donor functionalities of the dcbpy ligands; the dcbpy ligands act as structural pillars that form the overall 3D topology of this MOF. Fig. 1b

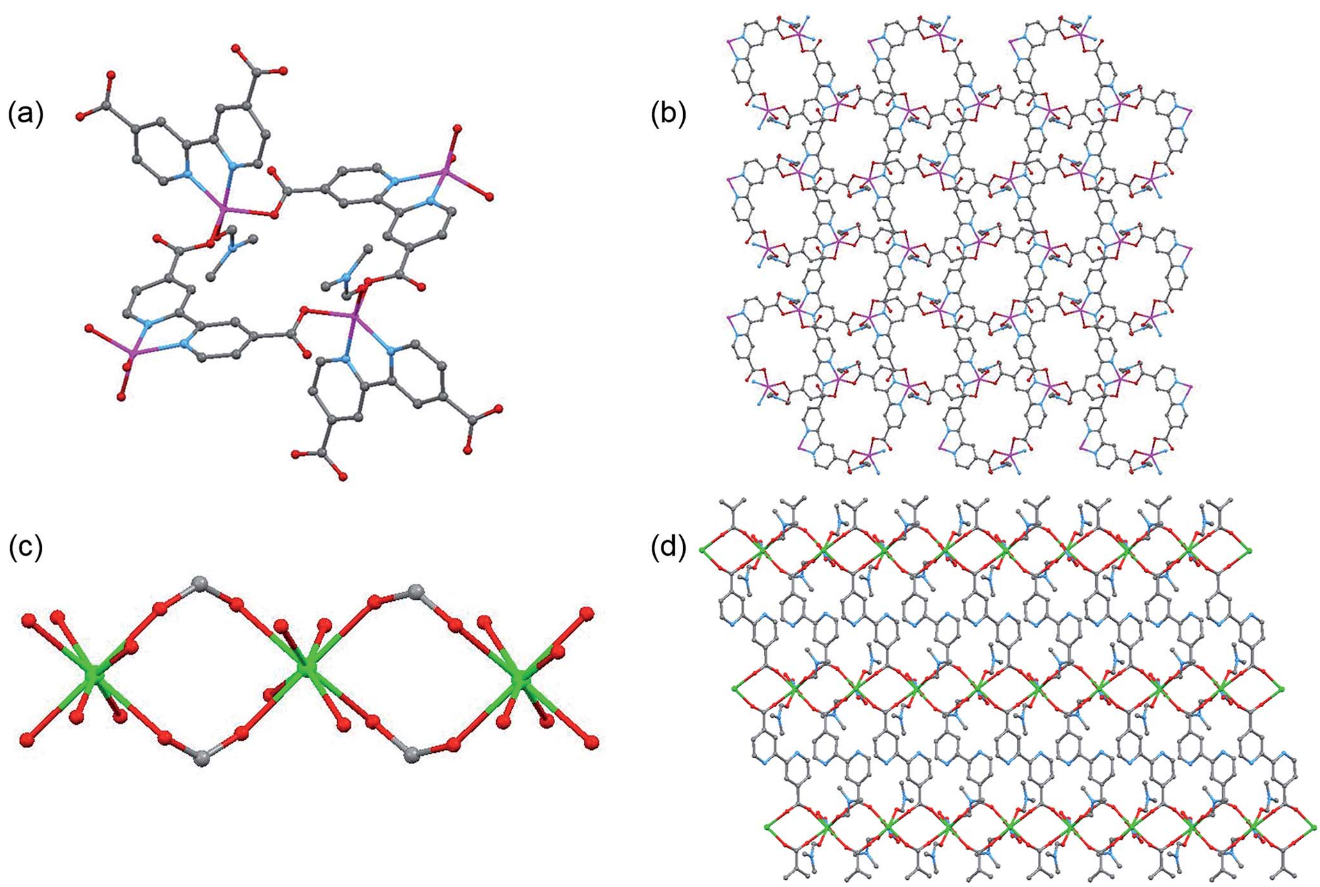

Fig. 1 (a) Representation of the cyclic 8-membered ring secondary building units (SBUs) located in MOF **1**. (b) Illustration of the overall 3D topology of MOF **1** as viewed along the crystallographic *a*-axis. Solvent molecules and hydrogen atoms have been omitted for clarity. (c) Representation of the SBUs found in MOF **2**. (d) Overall topology of MOF **2** as viewed along the crystallographic *a*-axis. Hydrogen atoms have been omitted for clarity. In the crystallographic representations of the MOFs, oxygen atoms are denoted by the colour red, carbon atoms grey, nitrogen atoms blue, zinc atoms pink and dysprosium atoms are green.

shows that ovaloid one-dimensional channels that are approximately 10.0 Å × 8.8 Å wide run throughout the structure of this framework. From the crystallographic data, it was found that DMF solvent molecules reside within the cavities of MOF **1** (although these have been omitted from the representation given in Fig. 1b, for clarity).

Single crystal X-ray diffraction confirmed the structure of 3D MOF **2** to be in the triclinic space group $P\bar{1}$. The secondary building units (SBUs) contained within this framework are significantly different to those of **1**, and are constructed from three dysprosium metals, the monodentate carboxylates of six dcbpy ligands, four DMF solvent molecules and two nitrate molecules (Fig. 1c). The dcbpy ligands act as pillars to other SBUs, forming one-dimensional chains that run throughout the three-dimensional structure of this MOF (Fig. 1d).

Space filling diagrams of **2** indicated this MOF has minimal porosity, thus no solvent molecules are able to permanently reside in the pores of this MOF, unlike in MOF **1** (ESI†).

Powder X-ray diffraction analysis (PXRD) of the synthesised bulk MOF **1** and **2** samples was in good agreement with the simulated PXRD patterns (as obtained from single crystal data), confirming the homogeneity of the synthesised materials (Fig. 2). Additionally the PXRDS of the microwave synthesised microcrystals of **1M** are also in accordance with that of the simulated **1** PXRD pattern, verifying that [Zn(dcbpy)(DMF)]·DMF was successfully yielded with microwave synthesis. PXRD patterns of MOFs **1**′ and **1M**′ demonstrated some distortions in the activated MOF frameworks as compared to the synthesised **1** and **1M** materials, this is most likely an artefact of DMF solvent loss. MOF **2**′ was observed to lose some crystallinity post activation.

Scanning electron microscopy images of the crystalline materials of **1** and **1M** are illustrated in Fig. 3. The crystals present in these solvothermally synthesised sample **1** (Fig. 3a) demonstrate a wide range of crystal sizes and shapes. The SEM images of **1M** (Fig. 3b and c) on the other hand demonstrate excellent uniformity amongst crystals. The microcrystals appear to be of leaf like resemblance with dimensions of approximately 25 μm × 10 μm × 2 μm.

3.2 Fluorescence sensing

MOFs **1**, **1M** and **2** were tested for their ability to act as sensory materials to TNT derivatives: 2,4-dinitrotoluene (2,4-DNT), *para*-nitrotoluene (*p*-NT) and nitrobenzene (NB), as well as plastic explosive taggant 2,3-dimethyl-2,3-dinitrobutane (DMNB). Due to the need for new portable, standoff, vapour phase methods for the detection of explosives, the sensing capabilities of the MOFs were assessed with the analytes in the gas phase, rather than the typical solution-based sensing reported extensively in the literature.[1]

Fluorescence quenching is attributed to photo-induced electron transfer between the excited state of the highly

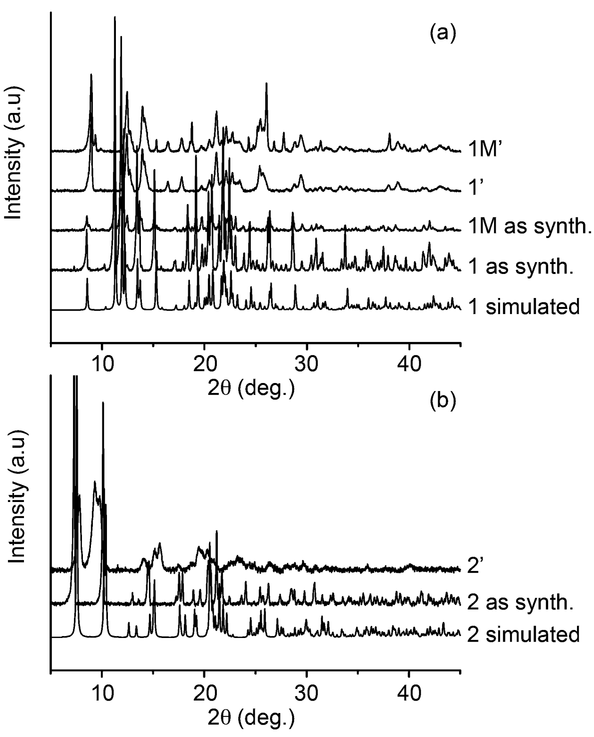

Fig. 2 (a) An overlay of powder X-ray diffraction patters of the simulated **1** structure (as obtained from single crystal X-ray diffraction data), an as synthesised **1** bulk sample, an as synthesised bulk **1M** sample, and washed **1**′ and **1M**′ samples. (b) An overlay of PXRD patterns of the simulated MOF **2** structure (as obtained from single crystal X-ray diffraction data), an as synthesised bulk **2** and washed **2**′ samples.

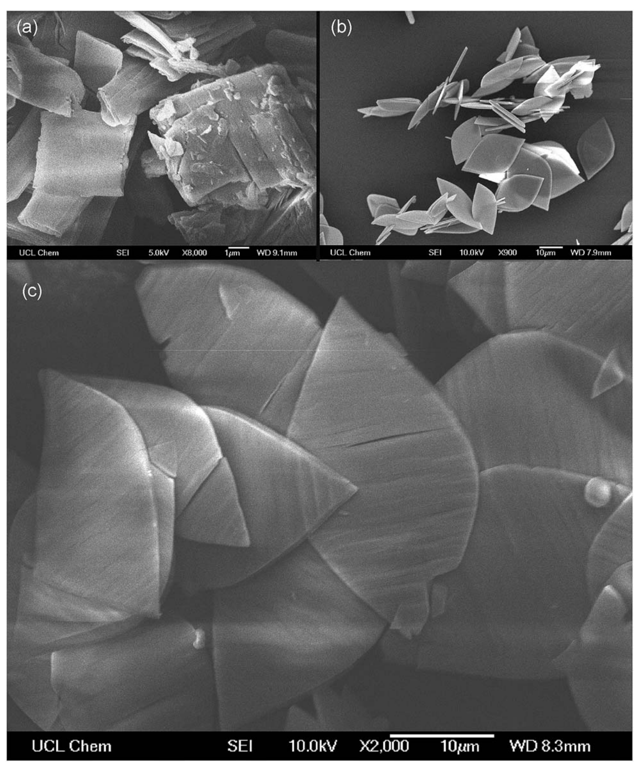

Fig. 3 Scanning electron microscopy images of (a) a sample of solvothermally synthesised MOF **1** crystals. (b and c) A sample of microwave synthesied **1M** crystals.

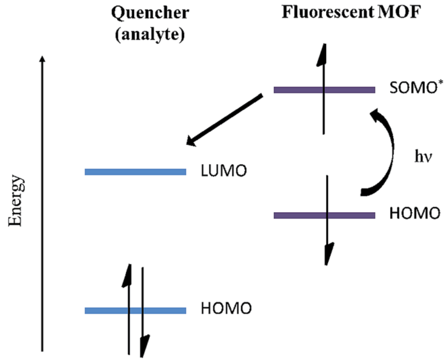

Fig. 4 Energy diagram representing the photo-induced electron transfer mechanism between MOFs in their excited state and explosive materials in the ground state (quenchers).[15]

fluorescent infinite metal–organic framework structures and the ground state of the explosive-related analytes.

Fig. 4 shows how the high-energy, singly occupied molecular orbital (SOMO*) of the electron rich fluorescent MOFs, is able to donate an electron into low-lying, lowest unoccupied molecular orbitals (LUMOs) of guest analytes (quenchers). Explosives and their related materials, particularly nitroaromatics, are highly electron deficient compounds with low-lying π^* orbitals (stabilised by the NO_2 groups through conjugation), thus they act as effective acceptors of the excited state electrons provided by the metal–organic frameworks (electron donors). Analytes with high-lying non-bonding orbitals of energy above the SOMO* of MOFs, are able to donate electrons into these orbitals leading to MOF fluorescence enhancement, this typically occurs for highly electron rich compounds. The amount of quenching or enhancement observed inherently depends on the strength of interaction between the frameworks and the analytes. The most important interactions are those, in which there is significant electron-donor/electron-acceptor orbital overlap.[15]

From the crystallographic data obtained for MOF **1**, it is known that solvent DMF molecules permanently reside in the cavities of this MOF. As the presence of solvent guest molecules in framework pores can limit response speed and intensities,[37] the crystalline material of MOF **1** and **1M** was washed (as described in Section 2.2). Washing regimes were also conducted on the crystals of **2**. The resultant active MOFs were designated **1′**, **1M′** and **2′**.

MOF **1′** was observed to demonstrate organic linker-based fluorescence emissions (ESI†). Fig. 5a shows the time dependent fluorescence quenching of **1′** by the analytes DMNB, 2,4-DNT, *p*-NT and NB. The figure shows the quenching percentages of the MOF upon exposure to the analytes as calculated by eqn (1) (I_0 = original peak maximum intensity; I = maximum intensity after exposure to analyte). The maximum intensities (I_0) were obtained from the fluorescence emission data, the wavelengths at which the I_0 occurred were the fixed points from which the maximum intensities after analyte exposure (I) were taken.

$$\text{Quenching } \% = \frac{I_0 - I}{I_0} \quad (1)$$

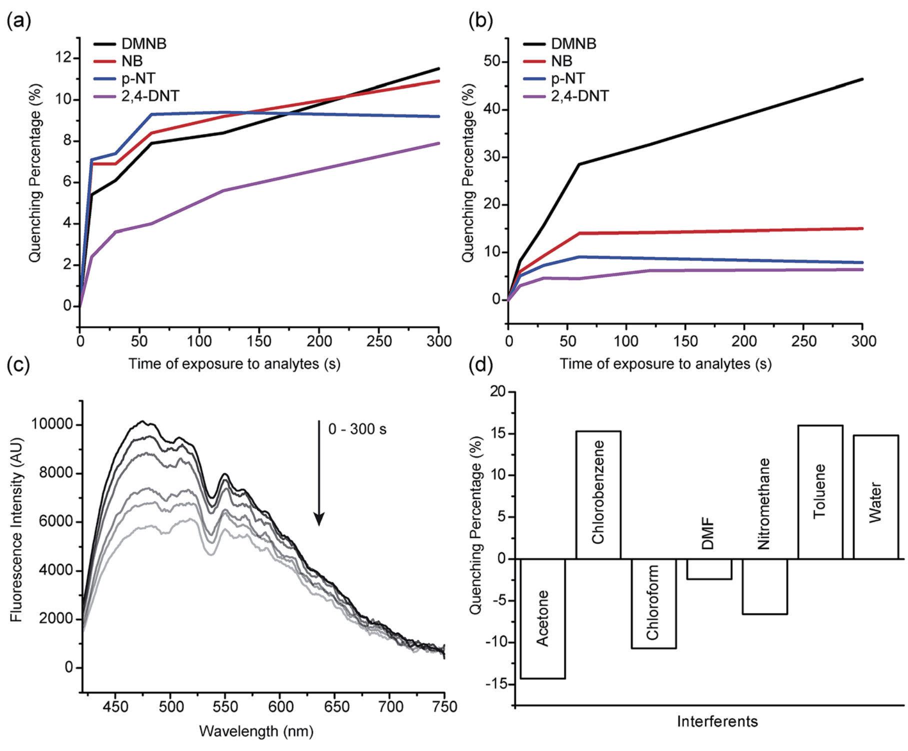

Fig. 5 (a) Fluorescence percentage quenching graphs for **1′** upon exposure to DMNB, NB, *p*-NT and 2,4-DNT. (b) Fluorescence percentage quenching graphs for **1M′** upon exposure to the same analytes. (c) Fluorescence emission profile for **1M′** upon exposure to DMNB for 0, 10 s, 30 s, 60 s, 120 s and 300 s. (d) Interference quenching percentages upon exposure to **1′** for 300 s.

The quenching percentages were found to follow the order of DMNB > NB > *p*-NT > 2,4-DNT and were 11.5%, 10.9%, 9.2% and 7.9% respectively, for 300 s of exposure. These results indicate **1′** has substantial potential as a sensory material for DMNB. This is of great significance as very few materials have been noted to detect this analyte particularly in the vapour phase,[37] ESI† Section 7 details the previously reported MOFs that have been able to detect this analyte in either vapour or solution phase. Such difficulty in detecting this analyte arises as a result of its unfavourable reduction potential coupled with its aliphatic structure that cannot form π–π interactions with the electron rich frameworks of the MOFs.

To gain further insight into the quenching process, we have calculated the geometry and electronic structure of **1** and the 6 analytes in Table 1. All our calculations were performed using the periodic density functional theory code VASP.[57] We utilized the PBE0 functional,[58] which has been shown to provide excellent descriptions of both solid state and molecular systems.[59,60] The ionization potential (IP) and electron affinity (EA) of **1** was calculated using the method recently developed by Butler *et al.*[61] Our PBE0 band gaps and HOMO–LUMO positions for the analytes are in excellent agreement with those calculated by Adamo and co-workers using the same functional but a different code.[62] These HOMO (IP) positions, however, are underestimated by approximately 1.6 eV compare to experimentally determined IPs.[63] Therefore in Fig. 6 we have used the experimental IPs for TNT, *p*-NT, 2,4-DNT and 2,6-DNT, combined with the PBE0 calculated HOMO–LUMO separation to yield the EA. For DMNB and NB, we have shifted our PBE0 calculated HOMO positions by 1.6 eV, with the EA determined as above.

Fig. 6 clearly demonstrates that based on the band edge positions of **1** *versus* the analytes, quenching should occur, as electrons in the SOMO of **1** should drop into the LUMO of each of the analytes. This analysis, however, does not explain the relative percentages shown in Fig. 5, as it cannot account for the effect of interactions between the molecules and the MOF.

The successful response of **1′** towards DMNB, and the other analytes can therefore be rationalised based on the topology of the metal–organic framework, namely the porosity of the MOF as well as analyte reduction potentials and vapour pressures. It is suggested that due to the MOF's porous nature, the analytes are able to penetrate into the fluorescent framework to a greater or lesser extent. NB and *p*-NT follow the expected order of potential and vapour pressure, and DNT has a low response due to it's low vapour pressure. The good response to DMNB suggests that it is able to penetrate the MOF more effectively, causing greater overall quenching.

An important consideration for materials that are to potentially be used in real world explosives detection applications is the effects of other analytes, interferents, on the sensing system. Thus, metal–organic framework **1′** was tested against the electron rich analytes toluene and chlorobenzene, nitroalphatic nitromethane, and solvents chloroform, acetone, water and DMF to investigate the effect of these on the fluorescence of this MOF, the results of which are summarised in Fig. 5d.

As expected the electron rich analytes enhanced the fluorescence of the MOF system, due to the donation of electrons

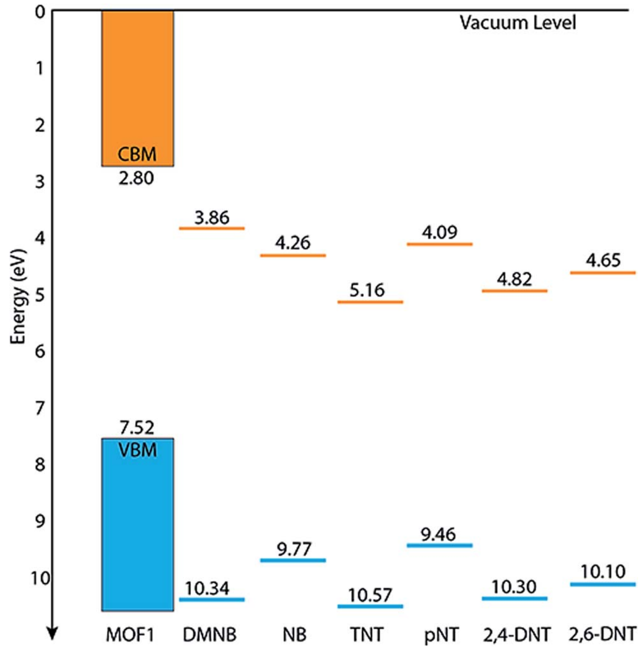

Fig. 6 Schematic of the PBE0 calculated valence band maximum (VBM) and conduction band minimum (CBM) positions for **1** and the IPs and EAs for the 6 analytes.

from the high-lying non-bonding orbitals of the analytes to the lower-lying the SOMO* of MOFs. Nitromethane gave a decrease in MOF fluorescence rationalised on the basis of being a nitro compound. Solvents acetone, chloroform and DMF were observed to decrease the fluorescence intensity of the system to varying extents. The detection of acetone by this system is of relevance as this analyte is often a constituent of home-made peroxide based explosives.

Thicker films of **1′** demonstrated limited responses upon exposure to the analytes, rationalised on the basis of restricted diffusion of the analytes into the MOF, in line with previous research.[37] (Representative example given in ESI.†)

In an attempt to increase the quenching percentage of MOF [Zn(dcbpy)(DMF)]·DMF towards DMNB an alternate method was employed for the synthesis of this MOF. To produce more uniform crystals with greater surface areas, a rapid microwave synthesis was applied. The crystalline material (**1M**) afforded by this synthesis (Fig. 3b and c) was washed to produce **1M′**, and tested for its sensing capabilities against the same analytes, results of which are given in Fig. 5b.

With more uniform crystals the sensitivity of the material towards DMNB is significantly enhanced (Fig. 5c), contending with some of the previously reported quenching percentages (ESI† Section 7). The quenching order of the other analytes follows that of **1′**, with quench percentages of 46.4%, 15%, 8% and 6.4% for DMNB, NB, *p*-NT and 2,4-DNT respectively. The maximum quenching for NB also appears enhanced. It is posited that the flatter and more uniform crystals give greater access to the material on the sensing substrate, improving responses.

MOF **2′** appears to also demonstrate linker-based emission (Fig. 7a) and not dysprosium metal emissions, evidenced by the absence of the characteristic Dy^{3+} peaks which are typically located at 475 nm, 570 nm, 660 nm and 750 nm respectively. We rationalize the absence of these peaks as a result of the inefficient charge transfer from the dcbpy ligands to the Dy^{3+}, due to the faster fluorescence emissions of the ligands in comparison to that of Dy^{3+}.

As shown by the quench percentage plots, (Fig. 7b) **2′** gives very different responses upon exposure to the analytes than **1′** and **1M′**.

MOF **2′** is only significantly quenched by analyte NB (13.1% quench) and arguably quenched by *p*-NT (3.1% quench), and demonstrates negligible response towards DMNB and 2,4-DNT. These results can be rationalized on the basis of the minimal porosity of **2′**. Owing to the absence of cavities within this framework, it is proposed that surface based interactions are the predominant cause of quenching for this MOF, unlike **1′** where analytes could penetrate into the MOF pores. Nitrobenzene, which has the highest vapour pressure of the analytes tested, appears to be able to form surface based interactions with the MOF during the testing time, yielding a detectable response. *p*-NT which also has a relatively high vapour pressure does not quench the system to a similar effect, and this is rationalised on the basis of its lower electron deficiency due to the presence of the CH_3 electron donating group on the molecule. DMNB and DNT, with the lowest vapour pressures of the tested analytes, are not able to adequately interact with the MOF and therefore give no response. These findings highlight the importance of porosity on a MOF sensing system.

To confirm the selective detection of the explosive analytes using MOFs **1′** and **2′** were an artefact of the highly electron rich extended MOF structures and not simple a result of analyte and free H_2dcbpy linker interactions, a proof of concept experiment was undertaken whereby H_2dcbpy was exposure to DMNB. Results showed no changes in the fluorescence intensity of the linker when exposure to the analyte for varying amounts of time (ESI†).

3.3 MOF-thin film recyclability

The thin films of **1′** were tested for their recyclability and results suggest this MOF to be regeneratable. A thin film was used for the sensing of NB (300 s) and then placed on a bench top at room temperature. The material was left for an hour and sensing was repeated (I_0 and $I_{300\ s}$ were taken). The same procedure was repeated after 3 and 16 hours of regeneration of the material at room temperature. As shown in Fig. 8 the material was still responsive to NB. Although I_0 values slightly decrease after the experiment at 1 h and 3 h, at 16 h of room temperature regeneration the material appears to start regaining its initial fluorescence intensity, and has a quenching percentage (9.4%) approaching the initial quenching response of this material at time = 0 h (10.9%). This suggests that not only is **1′** recyclable at room temperature, it is also not effected by typical moisture in the atmosphere within this timeframe. This is an important consideration for the use of this metal–organic framework as a sensory material for the detection of in field explosives. Further, previously reported recyclable MOF materials for explosives detection have only been achieved after heating samples at elevated temperatures (>150 °C)[37] which hinders the practical use of these materials, thus the regeneration of **1′** at room temperature is significant.

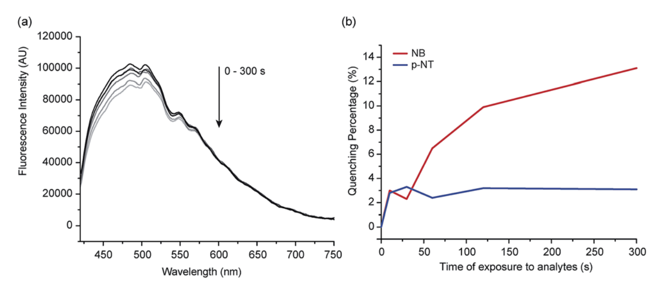

Fig. 7 (a) Fluorescence emission profile for **2′** upon exposure to nitrobenzene for 0 s, 10 s, 30 s, 60 s, 120 s, 300 s. (b) Quenching percentage plots of **2′** upon exposure to analytes NB and *p*-NT.

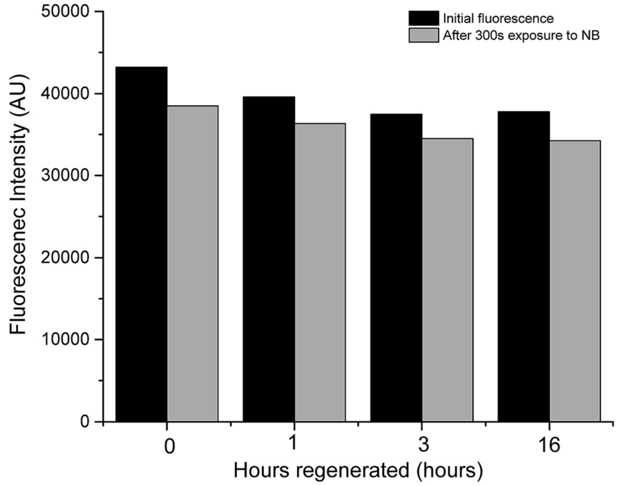

Fig. 8 Regeneration study conducted on **1′**. The graph shows the initial sensing of NB with **1′** and three cycles of sensing using the same sample towards the same analyte after 1, 3 and 16 hours regeneration at room temperature. At each time point the black bar indicates the initial fluorescence, and the grey bar the fluorescence after 300 s exposure to NB.

3.4 Thermal stability of MOFs 1′ and 2′

The thermal stability of active MOFs **1′** and **2′** was tested. Thermogravimetric analysis (TGA) of MOF **1′**, showed this framework to be stable up to 400 °C. MOF **2′** was observed to be stable up to 460 °C. These temperatures are comparable to those for other metal–organic frameworks synthesised for explosives detection.[37] Furthermore, the successful removal of DMF by the washing stage was confirmed by the absence of weight percentage loss at around 150 °C (ESI†).

4 Conclusions

In summary, two novel, highly fluorescent, metal–organic frameworks [Zn(dcbpy)(DMF)]·DMF (**1**) and [Dy(dcbpy)(DMF)$_2$-(NO_3)] (**2**) were synthesised for explosives detection applications. Both frameworks were constructed from the same linker ligand but varied in metal composition. Despite this, both demonstrated similar linker-based fluorescence. The frameworks were tested against explosives-related compounds DMNB, 2,4-DNT, *p*-NT and NB in the vapour phase, and exhibited very different responses.

Pourous MOF **1**′ was able to detect the challenging analyte DMNB, as well as NB, *p*-NT and 2,4-DNT. We attribute the successful detection of these analytes to their ability to be encapsulated into the framework cavities of MOF **1**′.

Non-porous MOF **2**′ was shown to be selective to the nitroaromatic compounds NB and *p*-NT.

The differences in sensing between these metal–organic frameworks were rationalized by the different nature of their overall framework architectures. This research highlights the importance that the topology of a system plays on its sensing capabilities. More specifically the importance of porosity on analyte detection. Through slight variations in one component of a MOF system, two very different structures can be made, greatly impacting on the selectivity of these MOFs towards explosive related compounds.

Further to this, uniform shape and sized microcrystals of [Zn(dcbpy)(DMF)]·DMF (**1M**) were synthesised rapidly using a microwave assisted method reducing syntheses time from days to minutes. These demonstrated greater sensitivities of quenching responses when exposed to DMNB and NB than the non-homogenous microcrystals of **1**′. Thus this paper also draws attention to the need for uniformity in crystals that are to be used as sensory materials.

The frameworks demonstrated high thermal stabilities and **1**′ was proven to be recyclable after regeneration at room temperature. These are both important factors in the application of these materials for in-field detection of explosives.

Crystal data for $C_{18}H_{20}N_4O_6Zn$ (M = 454.09 g mol^{-1}): monoclinic, space group $P2_1/n$ (no. 14), $a = 9.3725(2)$ Å, $b = 14.7643(3)$ Å, $c = 14.7153(3)$ Å, $\beta = 101.058(2)°$, $V = 1998.47(7)$ Å^3, $Z = 4$, $T = 150.00(10)$ K, μ(CuKα) = 2.090 mm^{-1}, D_{calc} = 1.509 g mm^{-3}, 14 313 reflections measured ($8.564 \le 2\theta \le 102.878$), 2158 unique ($R_{int} = 0.0590$, $R_{sigma} = 0.0321$) which were used in all calculations. The final R_1 was 0.0358 ($I > 2\sigma(I)$) and wR_2 was 0.0950 (all data).†

Crystal data for $C_{18}H_{20}DyN_5O_9$ (M = 612.89 g mol^{-1}): triclinic, space group $P\bar{1}$ (no. 2), $a = 9.2414(5)$ Å, $b = 10.3040(5)$ Å, $c = 12.8291(6)$ Å, $\alpha = 76.388(4)°$, $\beta = 69.431(4)°$, $\gamma = 86.377(4)°$, $V = 1111.37(10)$ Å^3, $Z = 2$, $T = 149.90(15)$ K, μ(CuKα) = 18.524 mm^{-1}, D_{calc} = 1.831 g mm^{-3}, 16 503 reflections measured ($8.832 \le 2\theta \le 149.79$), 4464 unique ($R_{int} = 0.0997$) which were used in all calculations. The final R_1 was 0.0557 ($I > 2\sigma(I)$) and wR_2 was 0.1540 (all data).†

Acknowledgements

This work was carried out under EPSRC grant no. EP/G037264/1 as part of the University College London Security Science Doctoral Training Centre. The UCL/Diamond work presented here made use of the UCL Legion HPC Facility, the IRIDIS cluster provided by the EPSRC funded Centre for Innovation (Grants No. EP/K000144/1 and No. EP/K000136/1), and the ARCHER supercomputer through support by the UK's HPC Materials Chemistry Consortium, which is funded by EPSRC Grant No. EP/L000202.

References

1 The Home Office, CONTEST: The United Kingdom's Strategy for Countering Terrorism, 2011.
2 J. M. Sylvia, J. A. Janni, J. D. Klein and K. M. Spencer, *Anal. Chem.*, 2000, **72**, 5834–5840.
3 J. I. Steinfeld and J. Wormhoudt, *Annu. Rev. Phys. Chem.*, 1998, **49**, 203–232.
4 R. O. Beauchamp, R. D. Irons, D. E. Rickert, D. B. Couch and T. E. Hamm, *CRC Crit. Rev. Toxicol.*, 1982, **11**, 33–84.
5 UNOC, United Nations Office of Drugs and Crime, *Convention on the marking of plastic explosives for the purpose of identification*, 1998.
6 M. Marshall and J. Oxley, *Aspects of explosives detection*, Elsevier, 2009.
7 R. J. Harper, J. R. Almirall and K. G. Furton, *Talanta*, 2005, **67**, 313–327.
8 D. S. Moore, *Rev. Sci. Instrum.*, 2004, **75**, 2499–2512.
9 R. G. Ewing, D. A. Atkinson, G. A. Eiceman and G. J. Ewing, *Talanta*, 2001, **54**, 515–529.
10 D. S. Moore and R. J. Scharff, *Anal. Bioanal. Chem.*, 2009, **393**, 1571–1578.
11 K. Brudzewski, S. Osowski and W. Pawlowski, *Sens. Actuators, B*, 2012, **161**, 528–533.
12 W. J. Peveler, R. Binions, S. M. V. Hailes and I. P. Parkin, *J. Mater. Chem. A*, 2013, **1**, 2613–2620.
13 R. G. Smith, N. D'Souza and S. Nicklin, *Analyst*, 2008, **133**, 571–584.
14 K. L. Diehl and E. V. Anslyn, *Chem. Soc. Rev.*, 2013, **42**, 8596–8611.
15 M. E. Germain and M. J. Knapp, *Chem. Soc. Rev.*, 2009, **38**, 2543–2555.
16 S. J. Toal and W. C. Trogler, *J. Mater. Chem.*, 2006, **16**, 2871–2883.
17 S. Shanmugaraju, S. A. Joshi and P. S. Mukherjee, *J. Mater. Chem.*, 2011, **21**, 9130–9138.
18 S. W. Thomas, J. P. Amara, R. E. Bjork and T. M. Swager, *Chem. Commun.*, 2005, 4572–4574.
19 J. R. Long and O. M. Yaghi, *Chem. Soc. Rev.*, 2009, **38**, 1213–1214.
20 J.-R. Li, R. J. Kuppler and H.-C. Zhou, *Chem. Soc. Rev.*, 2009, **38**, 1477–1504.
21 L. J. Murray, M. Dinca and J. R. Long, *Chem. Soc. Rev.*, 2009, **38**, 1294–1314.
22 J.-R. Li, J. Sculley and H.-C. Zhou, *Chem. Rev.*, 2012, **112**, 869–932.
23 J. S. Seo, D. Whang, H. Lee, S. I. Jun, J. Oh, Y. J. Jeon and K. Kim, *Nature*, 2000, **404**, 982–986.
24 J. Lee, O. K. Farha, J. Roberts, K. A. Scheidt, S. T. Nguyen and J. T. Hupp, *Chem. Soc. Rev.*, 2009, **38**, 1450–1459.
25 L. Ma, C. Abney and W. Lin, *Chem. Soc. Rev.*, 2009, **38**, 1248–1256.

26 P. Horcajada, T. Chalati, C. Serre, B. Gillet, C. Sebrie, T. Baati, J. F. Eubank, D. Heurtaux, P. Clayette, C. Kreuz, J.-S. Chang, Y. K. Hwang, V. Marsaud, P.-N. Bories, L. Cynober, S. Gil, G. Ferey, P. Couvreur and R. Gref, *Nat. Mater.*, 2010, **9**, 172–178.
27 P. Horcajada, C. Serre, M. Vallet-Regi, M. Sebban, F. Taulelle and G. Ferey, *Angew. Chem., Int. Ed.*, 2006, **45**, 5974–5978.
28 A. C. McKinlay, R. E. Morris, P. Horcajada, G. Ferey, R. Gref, P. Couvreur and C. Serre, *Angew. Chem., Int. Ed.*, 2010, **49**, 6260–6266.
29 R. C. Huxford, J. Della Rocca and W. Lin, *Curr. Opin. Chem. Biol.*, 2010, **14**, 262–268.
30 A. D. Burrows, M. Jurcic, L. L. Keenan, R. A. Lane, M. F. Mahon, M. R. Warren, H. Nowell, M. Paradowskic and J. Spencer, *Chem. Commun.*, 2013, **49**, 11260–11262.
31 Y. Cui, Y. Yue, G. Qian and B. Chen, *Chem. Rev.*, 2012, **112**, 1126–1162.
32 M. D. Allendorf, C. A. Bauer, R. K. Bhakta and R. J. T. Houk, *Chem. Soc. Rev.*, 2009, **38**, 1330–1352.
33 L. E. Kreno, K. Leong, O. K. Farha, M. Allendorf, R. P. Van Duyne and J. T. Hupp, *Chem. Rev.*, 2012, **112**, 1105–1125.
34 B. D. Chandler, D. T. Cramb and G. K. H. Shimizu, *J. Am. Chem. Soc.*, 2006, **128**, 10403–10412.
35 H. Ostmark, S. Wallin and H. G. Ang, *Propellants, Explos., Pyrotech.*, 2012, **37**, 12–23.
36 Z. Hu, B. J. Deibert and J. Li, *Chem. Soc. Rev.*, 2014, **43**, 5815–5840.
37 A. Lan, K. Li, H. Wu, D. H. Olson, T. J. Emge, W. Ki, M. Hong and J. Li, *Angew. Chem., Int. Ed.*, 2009, **48**, 2334–2338.
38 B. Gole, A. K. Bar and P. S. Mukherjee, *Chem.–Eur. J.*, 2014, **20**, 2276–2291.
39 G.-Y. Wang, L.-L. Yang, Y. Li, H. Song, W.-J. Ruan, Z. Chang and X.-H. Bu, *Dalton Trans.*, 2013, **42**, 12865–12868.
40 G.-Y. Wang, C. Song, D.-M. Kong, W.-J. Ruan, Z. Chang and Y. Li, *J. Mater. Chem. A*, 2014, **2**, 2213–2220.
41 D. Ma, B. Li, X. Zhou, Q. Zhou, K. Liu, G. Zeng, G. Li, Z. Shi and S. Feng, *Chem. Commun.*, 2013, **49**, 8964–8966.
42 A. K. Chaudhari, S. S. Nagarkar, B. Joarder and S. K. Ghosh, *Cryst. Growth Des.*, 2013, **13**, 3716–3721.
43 Y. Yuan, W. Wang, L. Qiu, F. Peng, X. Jiang, A. Xie, Y. Shen, X. Tian and L. Zhang, *Mater. Chem. Phys.*, 2011, **131**, 358–361.
44 S. S. Nagarkar, B. Joarder, A. K. Chaudhari, S. Mukherjee and S. K. Ghosh, *Angew. Chem., Int. Ed.*, 2013, **52**, 2881–2885.
45 R. Li, Y.-P. Yuan, L.-G. Qiu, W. Zhang and J.-F. Zhu, *Small*, 2012, **8**, 225–230.
46 S.-R. Zhang, D.-Y. Du, J.-S. Qin, S.-J. Bao, S.-L. Li, W.-W. He, Y.-Q. Lan, P. Shen and Z.-M. Su, *Chem.–Eur. J.*, 2014, **20**, 3589–3594.
47 T. K. Kim, J. H. Lee, D. Moon and H. R. Moon, *Inorg. Chem.*, 2013, **52**, 589–595.
48 S. Zhang, L. Han, L. Li, J. Cheng, D. Yuan and J. Luo, *Cryst. Growth Des.*, 2013, **13**, 5466–5472.
49 H. Xu, F. Liu, Y. Cui, B. Chen and G. Qian, *Chem. Commun.*, 2011, **47**, 3153–3155.
50 S.-B. Ding, W. Wang, L.-G. Qiu, Y.-P. Yuan, F.-M. Peng, X. Jiang, A.-J. Xie, Y.-H. Shen and J.-F. Zhu, *Mater. Lett.*, 2011, **65**, 1385–1387.
51 X.-H. Zhou, L. Li, H.-H. Li, A. Li, T. Yang and W. Huang, *Dalton Trans.*, 2013, **42**, 12403–12409.
52 X. Zhou, H. Li, H. Xiao, L. Li, Q. Zhao, T. Yang, J. Zuo and W. Huang, *Dalton Trans.*, 2013, **42**, 5718–5723.
53 J.-J. Qian, L.-G. Qiu, Y.-M. Wang, Y.-P. Yuan, A.-J. Xie and Y.-H. Shen, *Dalton Trans.*, 2014, **43**, 3978–3983.
54 O. V. Dolomanov, L. J. Bourhis, R. J. Gildea, J. A. K. Howard and H. Puschmann, *J. Appl. Crystallogr.*, 2009, **42**, 339–341.
55 L. Palatinus and G. Chapuis, *J. Appl. Crystallogr.*, 2007, **40**, 786–790.
56 A. L. Spek, *Acta Crystallogr., Sect. D: Biol. Crystallogr.*, 2009, **65**, 148–155.
57 G. Kresse and J. Furthmüller, *Phys. Rev. B: Condens. Matter Mater. Phys.*, 1996, **54**, 11169–11186.
58 C. Adamo and V. Barone, *J. Chem. Phys.*, 1999, **110**, 6158–6170.
59 D. O. Scanlon and G. W. Watson, *J. Mater. Chem.*, 2012, **22**, 25236–25245.
60 V. Wathelet, J. Preat, M. Bouhy, M. Fontaine, E. A. Perpte, J.-M. Andr and D. Jacquemin, *Int. J. Quantum Chem.*, 2006, **106**, 1853–1859.
61 K. T. Butler, C. H. Hendon and A. Walsh, *J. Am. Chem. Soc.*, 2014, **136**, 2703–2706.
62 G. Fayet, P. Rotureau, L. Joubert and C. Adamo, *J. Hazard. Mater.*, 2009, **171**, 845–850.
63 M. Qasim, Y. Kholod, L. Gorb, D. Magers, P. Honea and J. Leszczynski, *Chemosphere*, 2007, **69**, 1144–1150.

